Titre: Title:	Thermodynamic behavior of the τ_{11}-$Al_4Fe_{1.7}Si$ solid solutions from 0 K to 1270 K
Auteurs: Authors:	Paul Lafaye, Javier Jofré, & Jean-Philippe Harvey
Date:	2025
Type:	Article de revue / Article
Référence: Citation:	Lafaye, P., Jofré, J., & Harvey, J.-P. (2025). Thermodynamic behavior of the τ_{11}-$Al_4Fe_{1.7}Si$ solid solutions from 0 K to 1270 K. Journal of Solid State Chemistry, 346, 125257 (8 pages). https://doi.org/10.1016/j.jssc.2025.125257

Titre de la revue: Journal Title:	Journal of Solid State Chemistry (vol. 346)
Maison d'édition: Publisher:	Academic Press
URL officiel: Official URL:	https://doi.org/10.1016/j.jssc.2025.125257

Journal of Solid State Chemistry 346 (2025) 125257

Contents lists available at ScienceDirect

Journal of Solid State Chemistry

journal homepage: www.elsevier.com/locate/yjssc

Thermodynamic behaviour of the τ_{11}-$Al_4Fe_{1.7}Si$ solid solutions from 0 K to 1270 K

P. Lafaye *, J. Jofre, J.-P. Harvey

CRCT- Polytechnique Montréal, Chem. Eng., Box 6079, Station Downtown, Montréal, Qc, Montréal, H3C 3A7, Canada

ARTICLE INFO

Keywords:
τ_{11}-$Al_4Fe_{1.7}Si$
Crystal chemistry
Short-range ordering
Sublattice model

ABSTRACT

This study discusses the atomic interactions between Al and Si in the mixed sites of the τ_{11}-$Al_4Fe_{1.7}Si$ solid solution structure, with respect to chemical composition and temperature. We first investigated the crystal structure of the τ_{11}-$Al_4Fe_{1.7}Si$ solid solution using Density Functional Theory (DFT), confirming recent findings suggesting significant changes to the solution structure. Subsequently, we quantified the 0 K short-range ordering (SRO) in the structure by analysing the coordination polyhedra of the mixed sites and calculating the energies of structures with mixed Al/Si occupations. Our results indicate that the SRO contribution can be neglected. In addition, we generated all the end-members corresponding to the substitution of Al by Si on the mixed sites of the structure and considering site 2*d* as occupied by Fe or vacant. We calculated the formation enthalpies of these end-members by DFT and determined their isobaric heat capacities by using a Debye–Wang model together with the DFT calculations of their equation of state. Using these calculations, we determined Si site fractions over a temperature range from 0 K to the decomposition temperature of the solid solution, applying a model derived from the Bragg–Williams approximation. Our findings enable us to propose reliable sublattice model for the solid solution, which differ significantly from existing models in the literature.

1. Introduction

Aluminium world production currently exceeds 100 million metric tonnes per year [1,2]. This volume of primary aluminium production using the conventional Hall–Heroult/carbon anode smelting process is necessarily accompanied by significant greenhouse gas (GHG) emissions which need to be quantified. The aluminium industry is responsible for 15% of the GHG emissions of the industrial sector, and about 3% of total anthropogenic GHG emissions [1,3,4]. A drastic reduction in GHG emissions from this sector could be achieved by either systematically recycling aluminium alloys or by integrating a disruptive green technology such as the substitution of carbon-baked anodes by inert ones in the primary smelting process [5]. Indeed, recycling aluminium alloys requires 5% of the energy needed for their primary production [1,2,4] if remelting only is required to process the scrap material. Despite this, only 30% of the world's aluminium production originates from recycling [2], not only because of the growing demand for aluminium but also because of deficiencies in recycling infrastructures and the prohibitive energetic cost of purification processes [2,6,7].

As a simple rule of thumb, current aluminium alloy recycling processes are not effective in removing elements more chemically noble than aluminium (which impurities are called tramp elements) [6,8]. This list of impurity includes V, Mn, Mg, Ni, Pb, Zn, Cr, Cu, Fe and Si [9]. This is particularly challenging in the case of Fe and Si, since these elements are commonly found in steel and aluminium alloys which are nowadays routinely combined as body structure materials in cars. As an example, the Tesla Collision Repair Procedures Manual [10] reports the use of at least 3 distinct types of steel and 4 different aluminium alloys (both cast and wrought alloys). Without proper disassembling, shredding and sorting strategies, these elements will accumulate as recycling cycles of end-of-life products are performed, reaching impurity contents that allow the precipitation of various Fe- and Si-rich phases. Many of these undesired phases are likely to significantly compromise the mechanical properties of the aluminium alloys [11–14].

Until now, primary aluminium dilution strategies have been the most commonly used method of controlling the Fe and Si content of recycled alloys [14]. It is therefore crucial to consider new strategies, such as the development of impurity-tolerant alloys that can be recycled more easily [8,15,16]. To achieve this objective, we need to considerably improve our understanding of the thermodynamic behaviour of the Al-Fe-Si solid solutions, not only in their stability domains but also in their metastability ranges, in order to be able to predict their formation in the context of industrial alloys [2].

* Corresponding author.
E-mail address: paul.lafaye@polymtl.ca (P. Lafaye).

https://doi.org/10.1016/j.jssc.2025.125257
Received 12 November 2024; Received in revised form 10 February 2025; Accepted 12 February 2025
Available online 25 February 2025

The Compound Energy Formalism (CEF) [17] implemented in the CALculation of PHAse Diagram (CALPHAD) [18] method is specifically used to describe the thermodynamic behaviour of solid solutions, over a wide range of temperatures and chemical compositions that commonly exceed the solution's stability range. The CEF is based on the choice of a sublattice (SL) model that reflects the occupancy of the mixed sites in the solid solution: sites with comparable occupancy can be combined in a single SL. However, determining the occupancy of the mixed sites of solid solutions can be difficult, particularly when dealing with the Al-Fe-Si ternary system. The homogeneity range of the solid solutions of this system reflects the substitution of Al by Si on the mixed sites of the structure [19]. Unfortunately, these two elements cannot be distinguished by either X-ray diffraction or neutron diffraction. Only resonant diffraction method [20], which is challenging to use, can be employed to measure the occupancy of the mixed sites at a given temperature and chemical composition. However, no experimental technique can be considered to characterize the crystal chemistry of solid solutions over a whole range of temperatures, or outside their stability domains.

This problem can be circumvent with the use of atomistic simulations. Density Functional Theory (DFT) simulations coupled with a Bragg–Williams configurational entropy model [21] can be used to calculate the occupancy of mixed sites [22–24]. This methodology which requires considerable computational resources (even with modern supercomputers) has not been extensively applied up to now to help resolving the crystal chemistry of solid solutions in the CALPHAD community. For these reasons, the scientific literature shows a great diversity of SL models for the solid solutions of the Al-Fe-Si system [25,26]. Indeed, the thermodynamic model of the Al-Fe-Si ternary system proposed by Liu et al. [25] was built under the consideration that most solid phases are stoichiometric compounds, except for the $\tau 5$ and $\tau 6$ phases which were modelled as solid solutions. More recently, Du et al. [26] considered the Al-Fe-Si solid phases either as compounds or as ideal solutions. These are two extremes, since in one case the configurational entropy of the solutions is null, while it is maximal in the other. Apart from the absence of experimental data to define solubility ranges, no justification was provided at the time by these authors for the selection of these SL models. Despite the simplified description of many solid phases in these CALPHAD assessments, the thermodynamic models of these two authors have been used extensively in the literature [27–32].

In order to revisit the thermodynamic modelling of the Al-Fe-Si ternary system, we have initiated a series of investigations to systematically characterize the crystal chemistry of ternary solid solutions of the system [33,34]. This paper focuses on the τ_{11}-$Al_4Fe_{1.7}Si$ solid solution [35,36]. This phase is currently receiving renewed interest from the scientific community regarding its use as a structural material, potentially able to replace steel and titanium aluminides in selected applications [36–38]. To this end, Rijal et al. [36] and Soto-Medina et al. [37] have re-examined the crystal structure of this phase and studied its thermodynamic stability. These authors qualitatively described the crystal chemistry of the solution at 0 K and concluded that the solution is stabilized by entropy effects. However, these authors did not calculate the occupancy on the mixed sites and were therefore unable to quantify the solution configurational entropy of mixing. Moreover, these authors calculated the Gibbs energy of the solution at finite temperature in order to compare it with the Gibbs energies of the competing phases. To do this, they used the Kopp–Neumann approximation [39] which approximation has been shown to be particularly erroneous in the case of Al-rich intermetallic phases [40]. Finally, Soto-Medina et al. [37] used a configurational entropy model [41] different from the CEF [17], rendering their comparisons with existing Calphad databases (TCAL7) irrelevant. The determination of the thermodynamic stability of this solution as a function of temperature and chemical composition must therefore be reviewed.

In this contribution, we have studied the crystal chemistry of the τ_{11}-$Al_4Fe_{1.7}Si$ solid solution over a wide range of chemical composition, simulating the total substitution of Al by Si, and taking into account the partial occupation of the 2*d* site, from 0 K to 1270 K, the decomposition temperature of the solution according the reaction scheme proposed by Krendelsberger et al. [42]. To do this, we used a proven method [43] which involves calculating the enthalpy of formation and isobaric heat capacity of all structures resulting from the substitution of Al and Si on the mixed sites of the structure and considering site 2*d* as either occupied by Fe or vacant. In addition, the contribution of short-range order (SRO) was quantified at 0 K. Finally, the Bragg–Williams model was used to calculate the finite-temperature occupancy on the mixed sites of the structure and quantify the contribution of the configurational entropy of mixing. These results enabled us to deduce an optimal SL model for the solution.

2. Methodology

2.1. First-principles calculations

DFT calculations were carried out using the Vienna Ab initio Simulation Package (VASP) code [44]. The exchange–correlation effects were described using the Perdew–Burke–Ernzerhof (PBE) functional within the generalized gradient approximation (GGA) [45]. We employed a k-point grid of $15 \times 15 \times 13$ and a plane-wave cut-off energy of 600 eV to ensure high accuracy in representing the electronic structure. Projector Augmented Wave (PAW) pseudopotentials were utilized for Al, Fe, and Si [46]. Given the magnetic nature of Fe, spin-polarized calculations were performed. The lattice parameters and internal atomic positions were relaxed until the Hellmann–Feynman forces on each atom were reduced to less than 1 meV/$\AA$ to ensure equilibrium structures.

We have calculated the total energy of all the 16 structures generated by the occupation of Al or Si on sites 2*a*, $6h_1$ and 12*k* and by considering site 2*d* occupied by Fe or by vacancies. These structures are called end-members and are labelled A:B:C:D:E, indicating that site 2*a* is occupied by A atoms, site $6h_1$ by B atoms and so on, as shown in Table 1. The formation enthalpy of the considered structures can be evaluated by referring the calculated total energies with the total energies of pure elements in their reference states (i.e. Al in fcc structure, Fe in bcc structure and Si in $A4$ structure).

To evaluate the influence of the Short-Range Ordering (SRO) on the cohesive energy of this solid solution, several configurations involving the partial substitution of Al and Si on various atomic sites need to be considered. More specifically, all possible combinations of k atoms among n atomic positions requires the definition of ${}^nC_k$ distinct configurations. For this solid solution, the complete exploration of all the possible configurations would involve an unrealistically large number of DFT simulations. As a result, a defined subset of 100 configurations was randomly generated. This process was automated using FTCrystal software [47]. The contribution of the SRO to the enthalpy of the solid solution was quantified by comparing the average formation enthalpy of the partially substituted configurations with a linear combination of the formation enthalpy of the two end-members framing their chemical composition. This methodology was developed and tested in a previous work [34]. Note that the coordination polyhedron of the Al/Si mixed sites of the structure are represented in this paper. The detailed visualization of the local environments of sites 2*d* and $6h_2$ is reported in Supplementary Material.

2.2. Heat capacity calculations

For the calculation of the isobaric heat capacity of the τ_{11}-$Al_4Fe_{1.7}Si$ solid solution from 0 K to 1270 K, the Gibbs free energies of the end-members were computed. Only vibrational contributions were considered and calculated using the Debye model within the quasi-harmonic approximation (QHA) [48]. The Debye temperature in the vibrational free energy was determined using the Slater approximation [49], with a Poisson ratio of 0.24 used to calculate the speed of sound. The

Table 1
Crystal structure of the Al:Al:Al:Fe:Fe end-member of the τ_{11}-$Al_4Fe_{1.7}Si$ solution from our DFT calculations.

Wyckoff position	Occupation	x	y	z
$2a$	Al	0.0000	0.0000	0.0000
$6h_1$	Al	0.4661	0.5339	0.2500
$12k$	Al	0.1941	0.3883	0.9418
$2d$	Fe	0.3333	0.6667	0.2500
$6h_2$	Fe	0.1248	0.2495	0.2500

internal energy was described using a Birch–Murnaghan Equation Of State (EOS). The EOS was parametrized by fitting the energy versus volume curve to data obtained from ground-state DFT calculations performed with VASP [44]. The total energy was derived from isochoric deformations ranging from 0.95 to 1.05 times the equilibrium volume at 0 K in the NVT ensemble. The parameter adjustment was performed through residual minimization using a least-squares trust region reflective algorithm.

The equilibrium volume was determined by minimizing the free energy at zero pressure for temperatures ranging from 0 K to 1270 K. Once the equilibrium volume as a function of temperature was obtained, self-consistent temperature-dependent thermodynamic properties were derived by calculating the volume and temperature derivatives of the free energy.

2.3. Calculation of the occupancy factors

The Gibbs free energy of the τ_{11}-$Al_4Fe_{1.7}Si$ solid solution is determined at a given temperature using our DFT calculations of the formation enthalpy and isobaric heat capacity of the solution end-members by means of the CEF [17]:

$$\begin{aligned} G_{T_{11}}(T) = & \sum_{i,j,k=\mathrm{Al,Si}} \left[y_i^{2a} y_j^{6h_1} y_k^{12k} \right] \cdot \\ & \left(\Delta H_{ijk}(0\mathrm{K}) + \int_0^T C_P^{ijk}(T) dT \right. \\ & \left. - T \int_0^T \frac{C_P^{ijk}(T)}{T} dT \right) \\ & + RT \sum_{l=2a,6h_1,12k} a^l \cdot \sum_{j=\mathrm{Al,Si}} y_j^l \ln(y_j) \end{aligned} \quad (1)$$

y_j^l is the occupancy of the element j on site l, a^l is the multiplicity of site l, $H_{ijk}^{\tau_{11}}(\mathrm{T})$ is the formation enthalpy of the end-members calculated at finite temperature T by DFT in this work, R is the gas constant. This approximation assumes ideal mixing on each individual site, neglecting non-ideal contributions. Additionally, interactions between sublattices are not considered. For further details, readers are referred to [24] and for a comparison with other computational techniques, to [50].

3. Results and discussion

3.1. First-principles calculations

At first, it should be recalled that the τ_{11}-$Al_4Fe_{1.7}Si$ solid solution was initially refined by German et al. [35]. These authors reported an hexagonal structure, space group $P6_3/mmc$ (194) with five Wyckoff positions: positions $2a$, $6h_1$ and $12k$ are occupied by Al and Si atoms, positions $2d$ and $6h$ are occupied by Fe atoms. More recently, Rijal et al. [36] have revisited this structure by neutron diffraction and DFT calculations. These authors corrected the coordinates of the $6h_1$ position and showed that the $2d$ position is occupied by up to 45% of vacancies. The DFT calculations carried out in this work support the conclusions of Rijal et al. [36] concerning the coordinates of the $6h_1$ position. As an illustration, the Wyckoff position coordinates obtained in this work for the Al:Al:Al:Fe:Fe end-member are given in Table 1.

Table 2
Total energy (E_{tot}) and formation enthalpy (ΔH_f) of the τ_{11}-$Al_4Fe_{1.7}Si$ solid solution end members. The upper part includes end-members having site $2d$ occupied by Fe, while the bottom part is devoted to end-members having site $2d$ vacant. The total energy of the stable element under standard conditions (i.e. Al-FCC, Fe-BCC and Si-Diamond) are used as references to evaluate the enthalpy of formation.

Wyckoff position					E_{tot}	ΔH_f
$2a$	$6h_1$	$12k$	$2d$	$6h_2$	(eV)	(kJ mol-at^{-1})
Al	Al	Al	Fe	Fe	−149.887	−31.231
Si	Al	Al	Fe	Fe	−153.936	−35.306
Al	Si	Al	Fe	Fe	−160.145	−36.951
Si	Si	Al	Fe	Fe	−163.371	−38.193
Al	Al	Si	Fe	Fe	−168.447	−35.932
Si	Al	Si	Fe	Fe	−170.918	−34.572
Al	Si	Si	Fe	Fe	−175.100	−29.231
Si	Si	Si	Fe	Fe	−176.134	−22.918
Al	Al	Al	Va	Fe	−132.091	−28.723
Si	Al	Al	Va	Fe	−136.215	−33.392
Al	Si	Al	Va	Fe	−141.999	−33.587
Si	Si	Al	Va	Fe	−145.432	−35.689
Al	Al	Si	Va	Fe	−147.107	−20.636
Si	Al	Si	Va	Fe	−150.192	−21.449
Al	Si	Si	Va	Fe	−154.454	−15.995
Si	Si	Si	Va	Fe	−156.189	−11.798

The total energies and formation enthalpy of the end-members of the τ_{11}-$Al_4Fe_{1.7}Si$ solid solution are reported in Table 2.

We performed spin-polarized DFT calculations to account for potential magnetic ordering. However, our results show that all considered τ_{11}-$Al_4Fe_{1.7}Si$ solid solution end-members are non-magnetic, except for two specific cases where sites $2a$ and $6h_1$ and $12k$ are simultaneously occupied by Al (*i.e.*, the Al:Al:Al:Fe:Fe and Al:Al:Al:Va:Fe end-members). These two end-members exhibit a weak ferrimagnetic ordering, with total magnetic moments of 1.38 μB and 2.57 μB for the entire structure, respectively. Notably, at the same chemical composition, the stable phase is Al_5Fe_2 which is non-magnetic [51]. Thus, the magnetic contribution to the stability of the end-members is expected to be negligible. To confirm this hypothesis, additional non-spin-polarized DFT calculations were performed for these two end-members, revealing minor differences in formation enthalpy: 20 J.mol−at^{-1} for Al:Al:Al:Fe:Fe and 84 J.mol−at^{-1} for Al:Al:Al:Va:Fe. Therefore, the solid solution will be treated as non-magnetic throughout this article. In addition, it should be noted that our calculations show that the formation enthalpy of the τ_{11}-$Al_4Fe_{1.7}Si$ end-members at 0 K is consistently more negative (on an atomic basis) when Fe occupies site $2d$ compared to vacant site. However, it is very important to clarify at this stage that these results alone do not support any conclusions about the phase stability range. In particular, it would be erroneous to conclude that the phase homogeneity range exists for site $2d$ occupied by Fe. The existence of a stability domain results from the complex interaction between the Gibbs energies of all the competing phases in a given system. As a consequence, the minimum Gibbs energy of a system does not necessarily coincide with the minimum Gibbs energies of each phase. Moreover, it is important to keep in mind that configurational entropy of mixing can play a key role in stabilizing configurations with partial occupancy of site $2d$, which is consistent with experimental observations [19,36,37].

In this regard, recently published papers on the determination of the τ_{11}-$Al_4Fe_{1.7}Si$ solution homogeneity range were relying on comparisons between the Gibbs energy of the solution calculated by DFT at 0 K [36] and 1073 K [37] and those of all competing phases in the Al-Fe-Si system. Nevertheless, several reasons lead us to consider the study of Soto-Medina [37] as questionable. Indeed, these authors compared their calculated ab-initio based energies with the Gibbs free energy map obtained using thermodynamic models constructed via the classical CALPHAD method (TCAL7 database). However, the reliability of the TCAL7 database is disputable due to the following shortcomings: (1) the extensive use of the Kopp–Neumann approximation [39],

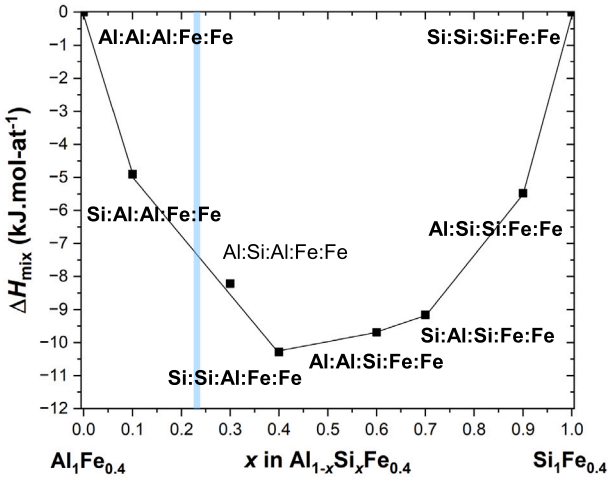

Fig. 1. Mixing enthalpy of the τ_{11}-$Al_4Fe_{1.7}Si$ solid solution calculated at 0 K with site 2*d* occupied by Fe atoms. References are $Al_1Fe_{0.4}$ and $Si_1Fe_{0.4}$. The blue band highlights the reported homogeneity range of the phase [19].

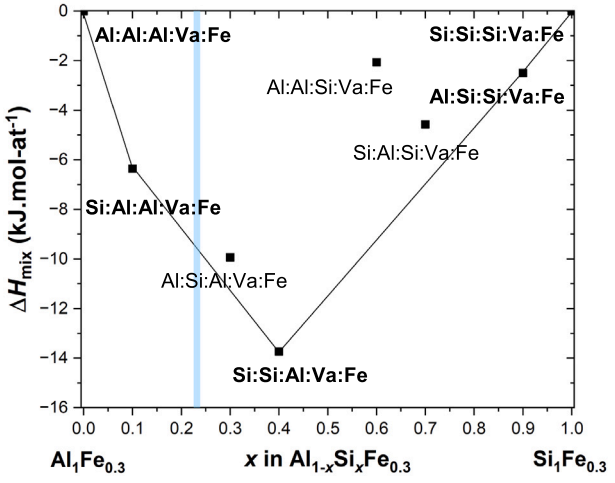

Fig. 2. Mixing enthalpy of the τ_{11}-$Al_4Fe_{1.7}Si$ solid solution calculated at 0 K with site 2*d* vacant. References are $Al_1Fe_{0.4}$ and $Si_1Fe_{0.4}$. The blue band highlights the reported homogeneity range of the phase [19].

which is particularly inaccurate for Al-based systems [40], and (2) the SL models of the Al-Fe-Si solid solutions designed for practical considerations rather than based on crystal chemistry data [33,34,52]. Furthermore, the configurational entropy model used by Soto-Medina et al. [37] is incompatible with those of the other solutions described in the TCAL7 database [17], further challenging the relevance of such comparisons. At last, it should be noted that no comparisons can be drawn between our calculations and those of Rijal et al. [36] and Soto-Medina et al. [37]. These authors did not report the total energy or the enthalpy of formation of their DFT calculations which prevent direct comparisons with the present work. To our knowledge, no other calculations are available in the literature for comparison.

Considering the binary end-members as enthalpy references, the mixing enthalpy of the solution can be calculated, as reported in Figs. 1 and 2. The *ground-state* of the solid solution is represented by the black line.

Figs. 1 and 2 reveal energetically favourable substitution of Al by Si and the resulting exothermic nature of the enthalpy of mixing of the τ_{11}-$Al_4Fe_{1.7}Si$ solid solution for both the crystal structure with Fe atoms on the 2d sites (Fig. 1) and the one with vacant 2d sites (Fig. 2). Mixing enthalpy minimums exceeding −10 kJ/mol-at are observed for both solid solutions. Another important observation concerns the nature of the solid solution substitution. In the case of site 2*d* occupied by Fe (Fig. 1), the *ground-state* calculated at 0 K shows that the substitution is initially sequential, with site 2*a* and then $6h_1$ progressively substituted by Si, until the minimum enthalpy of mixing of the solution is reached. On the other hand, for $x > 0.4$ (in $Al_{1-x}Si_xFe_{0.4}$), the substitution is irregular, with a progressive inversion of the occupation of sites 2*a* and $6h_1$ in favour of site 12*k*. A second irregularity can be observed between the end-members Si:Al:Si:Fe:Fe and Al:Si:Si:Fe:Fe. At this stage, we should wonder whether such irregularities result in occupancy reversals at 1270 K, the decomposition temperature of the solution, or whether the contribution of the configurational entropy of mixing on site 12*k* can favour direct substitution between the end-members Si:Al:Fe:Fe and Si:Si:Fe:Fe. In the case of the vacant site 2*d* (Fig. 2), the *ground-state* also shows the progressive substitution on sites 2*a* and then $6h_1$ until reaching the minimum mixing enthalpy. As in Fig. 1, the substitution becomes irregular for $x > 0.4$ (in $Al_{1-x}Si_xFe_{0.3}$) with a reversal of the occupancy of sites 2*a* and 12*k*. However, as the *ground-state* of the solution for $x > 0.4$ (in $Al_{1-x}Si_xFe_{0.3}$) is only weakly convex, it is clear that the effect of the configurational entropy of mixing on site 12*k* will lead to direct substitution between Si:Si:Al:Va:Fe and Si:Si:Si:Va:Fe end-members. The effect of temperature will therefore result in a substitution sequence from 2*a*, $6h_1$ to 12*k*.

3.2. Short-range order

To quantify the SRO in complex solid solutions, we have initially treated the mixed crystal sites as independent. For sites sharing atomic positions on their coordination polyhedron, configurations with partial substitutions are generated and compared to the ideal mixing energies of the site. In the next step, we account for all atomic positions of the mixed sites, allowing for simultaneous partial substitutions on multiple sites to capture collective interactions that may lead to SRO. Interestingly, when there are significant enthalpy differences between the *ground-state* and the other solution end-members, and substitution occurs sequentially, simultaneous occupancy of multiple sites becomes unlikely. However, this does not apply to the τ_{11}-$Al_4Fe_{1.7}Si$ solid solution, where sites 2*a*, $6h_1$, and 12*k* exhibit simultaneous mixed Al/Si occupancy for $x > 0.4$ (in $Al_{1-x}Si_xFe_{0.4}$). This irregularity is even more pronounced when site 2*d* is occupied by Fe rather than vacant. Additionally, the homogeneity range of the solution corresponds to Fe predominantly occupying site 2*d*. Consequently, we have decided to limit our study to the structure with Fe on site 2*d*, assuming that the conclusions drawn can be generalized to cases where this site is only partially occupied by Fe.

The coordination polyhedra of sites 2*a*, $6h_1$ and 12*k* of the τ_{11}-$Al_4Fe_{1.7}Si$ structure are shown in Figs. 3, 4, and 5, respectively. The coordination polyhedra and atoms of sites 2*a*, $6h_1$ and 12*k* are distinguished by colours: blue, white and red, respectively. Note that each of the three sites has a coordination number of 12 (CN 12).

Figs. 3 and 4 show that sites 2*a* and $6h_1$ share no atomic position on their coordination polyhedra. These sites cannot therefore contribute to a potential SRO. Fig. 5 show that site 12*k*, on the other hand, has three atoms belonging to this Wyckoff position on its coordination polyhedron. The potential contribution of SRO needs to be evaluated for this site. To achieve this, we generated the $^{12}C_6 = 924$ configurations resulting from the distribution of 50% Si and 50% Al on the atomic positions of the 12*k* site. From these 924 configurations, a random selection of 100 was made, and their enthalpies of formation were calculated using DFT. The formation enthalpy values of these 100 structures are very close to each other, with a standard deviation limited to 0.2 kJ/mol-at. The mean value of the formation enthalpy of the partially substituted structures have been plotted in Fig. 6 and compared with the linear combination of the formation enthalpy of the two end-members showing total occupancy of Al/Si on site 12*k*.

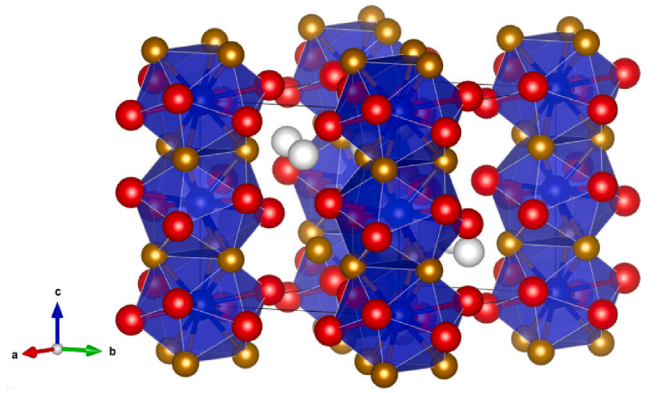

Fig. 3. Coordination polyhedra of site 2*a* of the τ_{11}-$Al_4Fe_{1.7}Si$ structure. Atoms and coordination polyhedron are represented in blue for site 2*a*, white for site 6h_1 and red for site 12*k*.

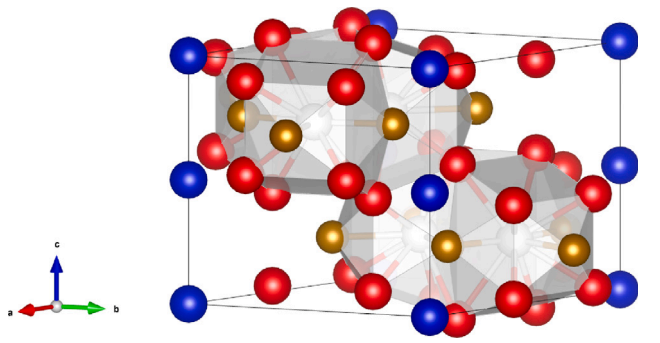

Fig. 4. Coordination polyhedra of site 6h_1 of the τ_{11}-$Al_4Fe_{1.7}Si$ structure. Atoms and coordination polyhedron are represented in blue for site 2*a*, white for site 6h_1 and red for site 12*k*.

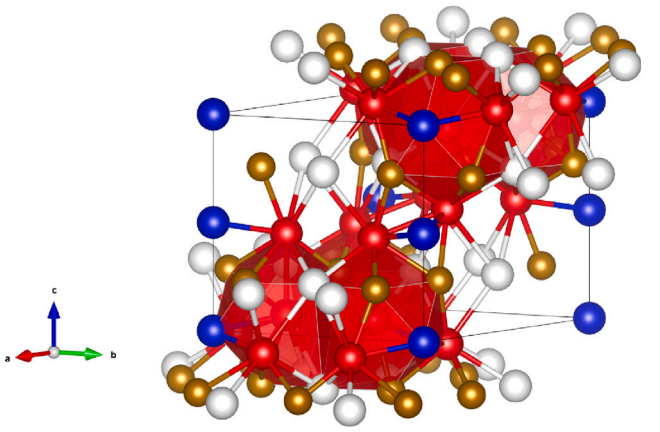

Fig. 5. Coordination polyhedra of site 12*k* of the τ_{11}-$Al_4Fe_{1.7}Si$ structure. Atoms and coordination polyhedron are represented in blue for site 2*a*, white for site 6h_1 and red for site 12*k*.

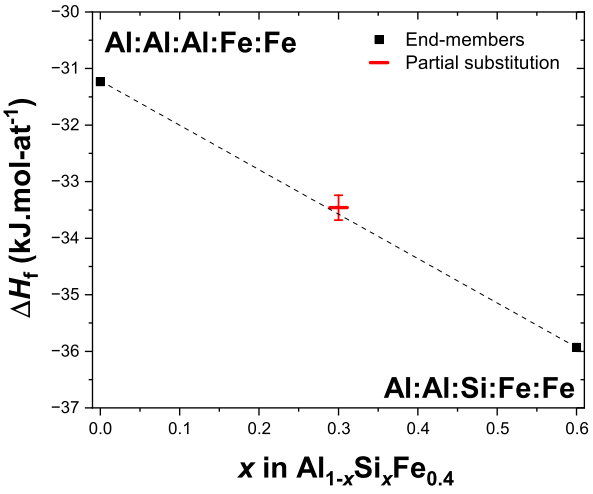

Fig. 6. Average enthalpy of formation of all structures with 50% Si partial substitution on the 12*k* Wyckoff position. The dotted line represents the enthalpy of formation resulting from ideal mixing on the 12*k* Wyckoff position.

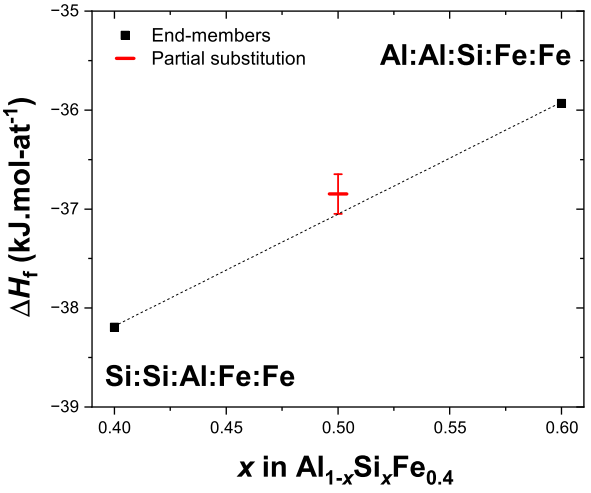

Fig. 7. Average enthalpy of formation of all structures with 50% Si partial substitution on the 12*k* Wyckoff position. The dotted line represents the enthalpy of formation resulting from ideal mixing on the 12*k* Wyckoff position.

From Fig. 6, we can note the minimal deviation between the formation enthalpy of the partially substituted structures and the one resulting from the ideal mixing. Thus, the contribution of SRO from this site can be considered as negligible.

Similarly, a hundred configurations were randomly selected from the $^{20}C_{10}$ configurations resulting from the distribution of 50% Si and 50% Al on the atomic positions of sites 2*a*, 6h_1 and 12*k*. Note that the enthalpy of formation values of these 100 structures are reasonably close to each other, with a standard deviation of 0.2 kJ/mol-at. The average enthalpy of formation of the structures is plotted in Fig. 7 in comparison with the linear combination of the formation enthalpy of the two end-members showing total Al/Si occupation on sites 2*a*, 6h_1 and 12*k*, forming the *ground-state* of the solution, namely the end-members Si:Si:Al:Fe:Fe and Al:Al:Si:Fe:Fe.

Although the number of configurations calculated is limited compared to the total number of possible configurations ($^{20}C_{10}$), the minimal energy difference between these configurations and the ideal mixing on these sites suggests a particularly weak SRO for this solution. Thus, from the DFT calculations conducted in this paper, we consider that the contribution of the SRO can be considered negligible in this solid solution, allowing the use of the Bragg–Williams configurational entropy model to describe its crystal chemistry [17].

3.3. Debye–wang model and Thermodynamic modelling

The isobaric heat capacity of each of the τ_{11}-$Al_4Fe_{1.7}Si$ solid solution end-member was predicted from 0 K to 1270 K using our DFT calculations using a Debye-like approach [48]. These calculations were used to parametrize heat capacity polynomial functions for all end-members, from 298 K up to 1270 K. Table 3 presents the obtained coefficients and

Table 3
Isobaric heat capacities (C_P) of the τ_{11}-$Al_4Fe_{1.7}Si$ solid solution end-members calculated from 298 K up to 1270 K. The values presented are the coefficients of the function $C_P = P_0 + P_1T + P_2T^{-2} + P_3T^2$.

Wyckoff position					Heat capacity, C_P (J/Kmol-at)			
$2a$	$6h_1$	$12k$	$2d$	$6h_2$	10	$10^{-3}T$	-10^5T^{-2}	$10^{-6}T^2$
Al	Al	Al	Fe	Fe	2.4452	2.3947	3.4198	0.5638
Si	Al	Al	Fe	Fe	2.4573	2.2705	3.5377	1.0353
Al	Si	Al	Fe	Fe	2.4331	2.5653	3.5866	0.4136
Si	Si	Al	Fe	Fe	2.4511	2.3634	3.7189	1.0699
Al	Al	Si	Fe	Fe	2.4377	2.5666	3.7693	0.7694
Si	Al	Si	Fe	Fe	2.4552	2.2706	3.8820	1.3433
Al	Si	Si	Fe	Fe	2.4511	2.3553	3.8107	1.1698
Si	Si	Si	Fe	Fe	2.4776	1.8804	3.7722	1.7644
Al	Al	Al	Va	Fe	2.4011	3.1190	4.2659	0.4822
Si	Al	Al	Va	Fe	2.4029	3.1088	4.3878	0.7065
Al	Si	Al	Va	Fe	2.3780	3.4454	4.4537	0.1659
Si	Si	Al	Va	Fe	2.3813	3.4362	4.5859	0.4727
Al	Al	Si	Va	Fe	2.4297	2.6504	4.3848	1.3382
Si	Al	Si	Va	Fe	2.4506	2.2081	4.5012	1.9374
Al	Si	Si	Va	Fe	2.3940	3.2373	4.3975	0.4974
Si	Si	Si	Va	Fe	2.4200	2.8269	4.3724	1.1032

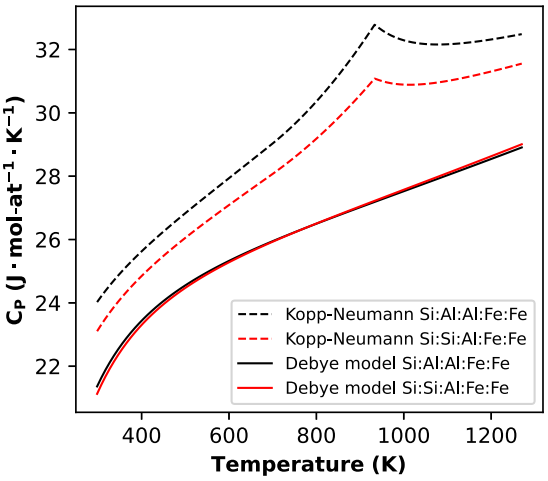

Fig. 8. Isobaric heat capacities (C_P) of the τ_{11}-$Al_4Fe_{1.7}Si$ solid solution end-members with site $2d$ occupied by Fe atoms, from 298 K to 1270 K. Calculations using the Debye model are shown in solid lines, and using Kopp–Newmann approximation are shown in dashed lines.

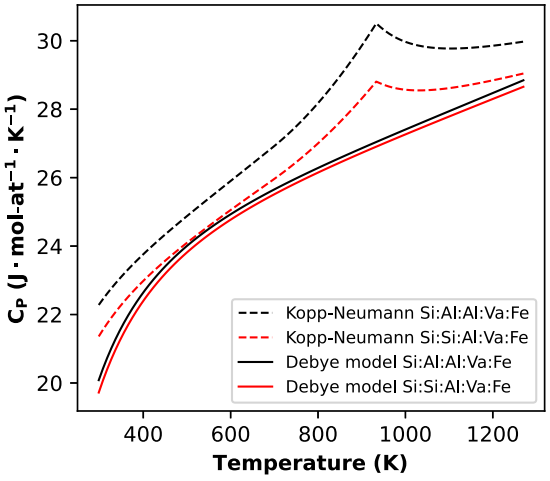

Fig. 9. Isobaric heat capacities (C_P) of the τ_{11}-$Al_4Fe_{1.7}Si$ solid solution end-members with site $2d$ occupied by Fe atoms, from 298 K to 1270 K. Calculations using the Debye model are shown in solid lines, and using Kopp–Newmann approximation are shown in dashed lines.

respective exponents. Such isobaric heat capacity polynomial functions are typically used in CALPHAD-like thermodynamic packages such as FactSage, ThermoCalc and Pandat.

In Figs. 8 and 9 are presented the heat capacities from 298 K to 1270 K of the end-members having the closest composition relative to the homogeneity range of the solution. The results are compared to heat capacities obtained using a weighted average of the elemental constituents, the Kopp–Neumann rule [39].

Although simple and straightforward, the Kopp–Neumann approximation leads to large discrepancies in the thermodynamic stability of the compounds compared to the heat capacities calculated using a Debye model. Integrating the heat capacities obtained with both approaches from 298 K to 1270 K quantifies the error in formation enthalpy variation caused by this rough approximation. The error in formation enthalpy variation is 3.4 kJ/mol-at for Si:Al:Al:Fe:Fe end-member, 2.9 kJ/mol-at for Si:Al:Al:Va:Fe end-member, 1.7 kJ/mol-at for Si:Si:Al:Fe:Fe end-member and 0.75 kJ/mol-at for Si:Si:Al:Va:Fe end-member. The error in formation enthalpy variation in the homogeneity range of the solid solution is around 2 kJ/mol-at. These results are consistent with our previous work on the $\tau 6$-$Al_9Fe_3Si_2$ and $\tau 8$-$Al_2Fe_3Si_4$ [33,34] solid solutions and show the inability of the Kopp–Neumann approximation to provide an accurate description of the heat capacity of Al-rich intermetallic phases.

The first-principles calculations presented in this study were used together with the Bragg–Williams configurational entropy model [17] to calculate, via the CEF, the Si fractions on sites $2a$, $6h_1$ and $12k$ of the structure with and without vacant $2d$ site, at 1270 K. The results of these calculations are reported in Figs. 10 and 11, respectively.

Figs. 10 and 11 illustrate the complexity of the thermodynamic behaviour of the τ_{11}-$Al_4Fe_{1.7}Si$ solution. Indeed, in the case of site $2d$ occupied by Fe, we can observe the reversal of the occupation on sites $2a$ and $6h_1$ in favour of site $12k$, as we postulated by analysing Fig. 1. This irregularity results in a pronounced disordering of the solid solution, which phenomenon is maximized around $x = 0.5$ (in $Al_{1-x}Si_xFe_{0.4}$). In the case of the vacant site $2d$, by contrast, the solution is clearly ordered, with a significant increase in Si occupancy on site $12k$ only observed once sites $2a$ and $6h_1$ are almost completely occupied by Si. This thermodynamic behaviour is more easily observed by analysing the configurational entropy of mixing of the solution, in the case of site $2d$ occupied by Fe or vacant, as shown in Figs. 12 and 13, respectively.

Fig. 12 shows a solid solution with only moderate ordering. The maximum entropy is observed around $x = 0.5$ (close to the near-crossing of the Si fraction curves) with a value of 4.1 J/K/mol-at to

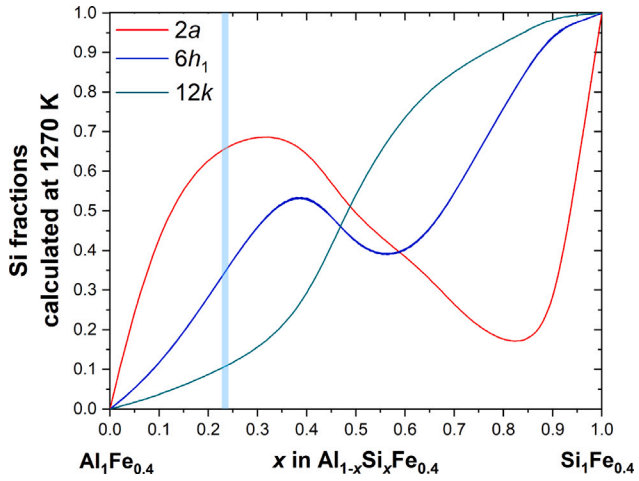

Fig. 10. Si site occupation factors in the τ_{11}-$Al_4Fe_{1.7}Si$ solid solution with site 2*d* occupied by Fe atoms, calculated at 1270 K. The blue band highlights the homogeneity range of the solid solution [19].

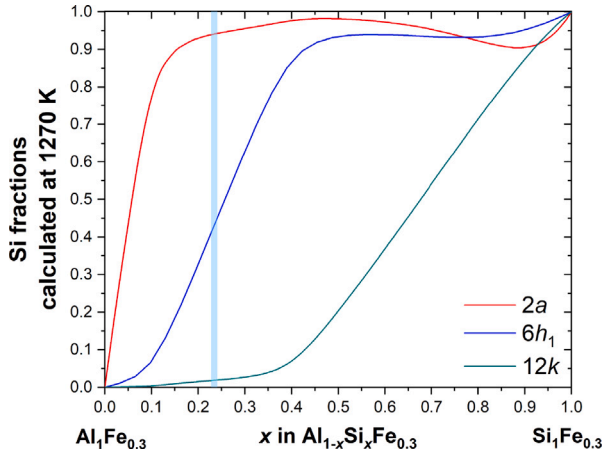

Fig. 11. Si site occupation factors in the τ_{11}-$Al_4Fe_{1.7}Si$ solid solution with site 2*d* vacant, at 1270 K. The blue band highlights the homogeneity range of the solid solution [19].

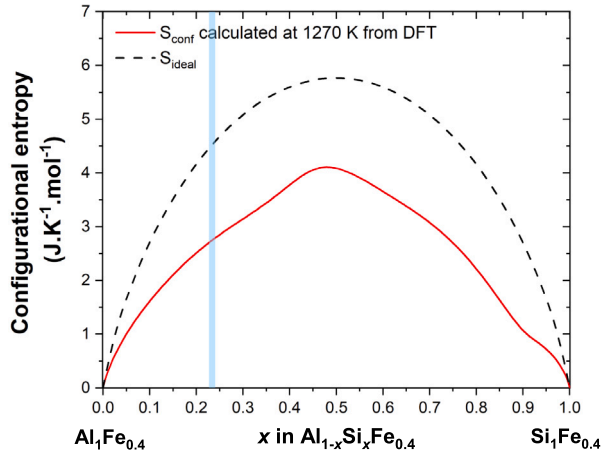

Fig. 12. Configurational entropy of the τ_{11}-$Al_4Fe_{1.7}Si$ solid solution with site 2*d* occupied by Fe atoms, calculated at 1270 K and compared to the entropy of an ideal solution. The blue band highlights the homogeneity range of the solid solution [19].

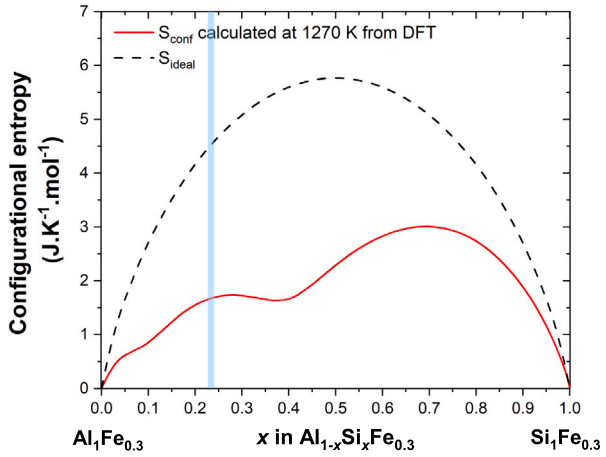

Fig. 13. Configurational entropy of the τ_{11}-$Al_4Fe_{1.7}Si$ solid solution with site 2*d* vacant, calculated at 1270 K and compared to the entropy of an ideal solution. The blue band highlights the homogeneity range of the solid solution [19].

be compared to 5.76 J/K/mol-at for an ideal solution. Fig. 13, on the other hand, shows a solution with more pronounced ordering.

On the basis of the occupancy data we have calculated in this study as well as the quantification of the configurational entropy of the τ_{11}-$Al_4Fe_{1.7}Si$ solution, it seems that no simple SL model can be proposed to describe its thermodynamic behaviour. We therefore recommend the use of the following SL model to accurately describe the thermodynamic behaviour of the solution: $(Al,Si)_2(Al,Si)_6(Al,Si)_{12}(Fe,Va)_2(Fe)_6$. This conclusion also highlights the inadequacy of the thermodynamic models of Liu et al. [25] and Du et al. [26] for characterizing the thermodynamic behaviour of this solution. Finally, the use of the Kopp–Neumann approximation should be avoided as we show that it leads to a selective overestimation of the thermodynamic stability of Al-rich end-members.

4. Conclusions

- The new crystal structure suggested by Rijal et al. [36] has been confirmed through the determination of new coordinates for the $6h_1$ Wyckoff position via DFT calculations.
- The SRO was determined to be negligible after comparing the average formation enthalpy of Al-Si partially substituted structures to linear combination of the formation enthalpy of the adjacent end-members.
- The Kopp–Neumann approximation is demonstrated to be inadequate for accurately describing the specific heat of Al-rich end-members of the solid solution.
- The configurational entropy of mixing calculated in this study highlights the inability of the SL models proposed by Liu et al. [25] and Du et al. [26] to accurately describe the ordering of the solution. A new and accurate SL model is proposed in this paper.

CRediT authorship contribution statement

P. Lafaye: Writing – review & editing, Writing – original draft, Methodology, Formal analysis, Data curation, Conceptualization. **J. Jofre:** Writing – review & editing, Writing – original draft, Methodology, Formal analysis, Data curation. **J.-P. Harvey:** Writing – review & editing, Writing – original draft, Methodology, Funding acquisition, Formal analysis, Data curation.

Declaration of competing interest

The authors declare that they have no known competing financial interests or personal relationships that could have appeared to influence the work reported in this paper.

Acknowledgements

This work was financially supported by the Professor Harvey Discovery Grant (RGPIN-2017-06168) (NSERC).

Funding support was obtained through the Alliance Grant (ALLRP 560998 - 20). Compute Quebec and Compute Canada are thanked for supplying the intensive calculation tools.

Appendix A. Supplementary data

Supplementary material related to this article can be found online at https://doi.org/10.1016/j.jssc.2025.125257.

Data availability

Data will be made available on request.

References

[1] International Aluminium Institute, (2020),
[2] D. Raabe, D. Ponge, P.J. Uggowitzer, M. Roscher, M. Paolantonio, C. Liu, H. Antrekowitsch, E. Kozeschnik, D. Seidmann, B. Gault, et al., Prog. Mater. Sci. 128 (2022) 100947.
[3] H. Ritchie, M. Roser, P. Rosado, Our World Data (2020).
[4] T.G. Gutowski, S. Sahni, J.M. Allwood, M.F. Ashby, E. Worrell, Philos. Trans. R. Soc. A: Math. Phys. Eng. Sci. 371 (1986) (2013) 20120003.
[5] J.-P. Harvey, W. Courchesne, M.D. Vo, K. Oishi, C. Robelin, U. Mahue, P. Leclerc, A. Al-Haiek, MRS Energy Sustain. 9 (2) (2022) 212–247.
[6] D. Raabe, C.C. Tasan, E.A. Olivetti, Nature 575 (7781) (2019) 64–74.
[7] M. Bertram, S. Ramkumar, H. Rechberger, G. Rombach, C. Bayliss, K.J. Martchek, D. Müller, G. Liu, Resour. Conserv. Recycl. 125 (2017) 48–69.
[8] G. Salloum-Abou-Jaoude, K.-H. Cheong, S. Akamatsu, P. Jarry, S. Bottin-Rousseau, TMS Annual Meeting & Exhibition, Springer, 2024, pp. 1048–1054.
[9] T.T. Cho, Y. Meng, S. Sugiyama, J. Yanagimoto, Int. J. Precis. Eng. Manuf. 16 (2015) 177–183.
[10] Tesla Inc., Model Y Collision Repair Procedures Manual, 2024, https://service.tesla.com/docs/BodyRepair/Body_Repair_Procedures/Model_Y/HTML/en-us/GUID-B4A61C9E-4CE2-4D9A-B9B3-B6D74EEFE038.html. (Accessed 22 October 2024).
[11] K. Nakajima, O. Takeda, T. Miki, K. Matsubae, S. Nakamura, T. Nagasaka, Environ. Sci. Technol. 44 (14) (2010) 5594–5600.
[12] H. Shen, W.D. Yang, H. Liang, G.C. Yao, Adv. Mater. Res. 295 (2011) 751–759.
[13] S. Bunkholt, E. Nes, K. Marthinsen, Mater. Charact. 129 (2017) 18–23.
[14] M.A. Dewan, M.A. Rhamdhani, J.B. Mitchell, C. Davidson, G.A. Brooks, M. Easton, J.F. Grandfield, Materials Science Forum, Vol. 693, Trans Tech Publ, 2011, pp. 149–160.
[15] B.K. Reck, T.E. Graedel, Science 337 (6095) (2012) 690–695.
[16] J.L. Cann, A. De Luca, D.C. Dunand, D. Dye, D.B. Miracle, H.S. Oh, E.A. Olivetti, T.M. Pollock, W.J. Poole, R. Yang, et al., Prog. Mater. Sci. 117 (2021) 100722.
[17] M. Hillert, J. Alloys Compd. 320 (2) (2001) 161–176.
[18] H. Lukas, S.G. Fries, B. Sundman, Computational Thermodynamics: The Calphad Method, Cambridge University Press, 2007.
[19] M.C. Marker, B. Skolyszewska-Kühberger, H.S. Effenberger, C. Schmetterer, K.W. Richter, Intermetallics 19 (12) (2011) 1919–1929.
[20] J.-L. Hodeau, V. Favre-Nicolin, S. Bos, H. Renevier, E. Lorenzo, J.-F. Berar, Chem. Rev. 101 (6) (2001) 1843–1868.
[21] W.L. Bragg, E.J. Williams, Proc. R. Soc. Lond. Ser. A, Contain. Pap. A Math. Phys. Character 145 (855) (1934) 699–730.
[22] P. Lafaye, K. Oishi, M. Bourdon, J.-P. Harvey, J. Alloys Compd. 920 (2022) 165779.
[23] P. Lafaye, C. Toffolon-Masclet, J.-C. Crivello, J.-M. Joubert, J. Nucl. Mater. 544 (2021) 152692.
[24] P. Lafaye, K. Oishi, J.-P. Harvey, J. Alloys Compd. 944 (2023) 169054.
[25] Z.-K. Liu, Y.A. Chang, Met. Mater. Trans. A 30 (1999) 1081–1095.
[26] Y. Du, J.C. Schuster, Z.-K. Liu, R. Hu, P. Nash, W. Sun, W. Zhang, J. Wang, L. Zhang, C. Tang, et al., Intermetallics 16 (4) (2008) 554–570.
[27] Q. Li, J. Wang, X. Liu, B. Wang, Mater. Charact. 198 (2023) 112752.
[28] M.R. Abul, R.F. Cochrane, A.M. Mullis, A. Nassar, J. Mater. Eng. Perform. (2023) 1–17.
[29] H. Liu, J. Pu, M. Wu, C. Zhang, J. Rao, W. Long, Y. Shen, Coatings 13 (9) (2023) 1590.
[30] B. Yuan, X. Deng, Z. Guo, S.K. Kolawole, C. Wu, H. Peng, Y. Liu, X. Su, J. Phase Equilibria Diffus. 45 (2) (2024) 114–131.
[31] X. Lan, Y. Xiao, B. Hu, M. Yang, Q. Wang, Q. Lu, T. Yang, K. Li, J. Wang, Z. Wang, et al., J. Mater. Res. Technol. 26 (2023) 260–266.
[32] L. Yang, X. Chen, Mater. Today Commun. 39 (2024) 109078.
[33] P. Lafaye, M.D. Vo, J. Jofre, J.-P. Harvey, Phys. Chem. Chem. Phys. 25 (29) (2023) 20015–20025.
[34] P. Lafaye, K. Poëti, J.-P. Harvey, Physica B 681 (2024) 415834.
[35] N. German, V. Belsky, T. Yanson, O. Zarechnyuk, Kristallografiya 34 (3) (1989) 735–737.
[36] B. Rijal, S. Soto, K. Parui, A. Sachdev, M.M. Butala, M.V. Manuel, R.G. Hennig, J. Alloys Compd. 902 (2022) 163141.
[37] S. Soto-Medina, B. Rijal, Y. Yang, L. Zhu, A.K. Sachdev, R.G. Hennig, M.V. Manuel, J. Alloys Compd. 978 (2024) 173207.
[38] Z. Liu, D.B. Haddad, T. Qi, Method of manufacturing a crystalline aluminum-iron-silicon alloy, 2021, US Patent 11, 085, 109, Google Patents.
[39] H. Kopp, Philos. Trans. R. Soc. Lond. (155) (1865) 71–202.
[40] J.-M. Joubert, B. Kaplan, M. Selleby, Calphad 81 (2023) 102562.
[41] O.F. Dippo, K.S. Vecchio, Scr. Mater. 201 (2021) 113974.
[42] N. Krendelsberger, F. Weitzer, J.C. Schuster, Met. Mater. Trans. A 38 (2007) 1681–1691.
[43] M.D. Vo, P. Lafaye, J. Jofre, J.-P. Harvey, J. Solid State Chem. 338 (2024) 124892.
[44] G. Kresse, J. Furthmüller, Phys. Rev. B 54 (16) (1996) 11169.
[45] J.P. Perdew, K. Burke, M. Ernzerhof, Phys. Rev. Lett. 77 (18) (1996) 3865.
[46] G. Kresse, D. Joubert, Phys. Rev. B 59 (3) (1999) 1758.
[47] K. Poëti, P. Lafaye, J. Jofre, J.-P. Harvey, Calphad (submitted for publication).
[48] J. Jofré, A.E. Gheribi, J.P. Harvey, Calphad 83 (2023) 102624.
[49] J.C. Slater, Introduction to Chemical Physics, Read Books Ltd, 2011.
[50] N. Dupin, S.G. Fries, J.-M. Joubert, B. Sundman, M. Sluiter, Y. Kawazoe, A. Pasturel, Phil. Mag. 86 (12) (2006) 1631–1641.
[51] M. Mihalkovič, M. Widom, Phys. Rev. B— Condens. Matter Mater. Phys. 85 (1) (2012) 014113.
[52] M. Ilatovskaia, H. Becker, O. Fabrichnaya, A. Leineweber, J. Alloys Compd. 936 (2023) 168361.